A kernel-based algorithm for the spectral fluence of clinical proton beams to calculate dose-averaged LET and other dosimetric quantities of interest

A. Bertolet
Department of Radiation Oncology, Hospital of The University of Pennsylvania, Philadelphia, PA, USA
Department of Atomic, Molecular and Nuclear Physics, Universidad de Sevilla, Seville, Spain

M. A. Cortés-Giraldo
Department of Atomic, Molecular and Nuclear Physics, Universidad de Sevilla, Seville, Spain

K. Souris
Center for Molecular Imaging and Experimental Radiotherapy, Université Catholique de Louvain, Louvain, Belgium

A. Carabe[a)]
Department of Radiation Oncology, Hospital of The University of Pennsylvania, Philadelphia, PA, USA

(Received 2 August 2019; revised 11 November 2019; accepted for publication 29 November 2019; published 31 March 2020)

Purpose: To introduce a new analytical methodology to calculate quantities of interest in particle radiotherapy inside the treatment planning system. Models are proposed to calculate dose-averaged LET (LETd) in proton radiotherapy.
Material and methods: A kernel-based approach for the spectral fluence of particles is developed by means of analytical functions depending on depth and lateral position. These functions are obtained by fitting them to data calculated with Monte Carlo (MC) simulations using Geant4 in liquid water for energies from 50 to 250 MeV. Contributions of primary, secondary protons and alpha particles are modeled separately. Lateral profiles and spectra are modeled as Gaussian functions to be convolved with the fluence coming from the nozzle. LETd is obtained by integrating the stopping power curves from the PSTAR and ASTAR databases weighted by the spectrum at each position. The fast MC code MCsquare is employed to benchmark the results.
Results: Considering the nine energies simulated, fits for the functions modeling the fluence in-depth provide an average R^2 equal to 0.998, 0.995 and 0.986 for each one of the particles considered. Fits for the Gaussian lateral functions yield average R^2 of 0.997, 0.982 and 0.993, respectively. Similarly, the Gaussian functions fitted to the computed spectra lead to average R^2 of 0.995, 0.938 and 0.902. LETd calculation in water shows mean differences of -0.007 ± 0.008 keV/μm with respect to MCsquare if only protons are considered and 0.022 ± 0.007 keV/μm including alpha particles. In a prostate case, mean difference for all voxels with dose >5% of prescribed dose is 0.28 ± 0.23 keV/μm.
Conclusion: This new spectral fluence-based methodology allows for simultaneous calculations of quantities of interest in proton radiotherapy such as dose, LETd or microdosimetric quantities. The method also enables the inclusion of more particles by following an analogous process. © *2020 American Association of Physicists in Medicine* [https://doi.org/10.1002/mp.14108]

Key words: analytical calculation, LETd, proton fluence algorithm, proton therapy

1. INTRODUCTION

Analytical pencil beam algorithms in proton therapy are now widely used and accepted as a reliable method for dose calculation due to their accuracy and computational efficiency.[1–3] This kind of algorithms use generally a model for the response (absorbed dose) for a proton beamlet, that is, a kernel, to be convolved with the input beam, computed from a source beam model.[4,5] Similarly, the kernel approach is also commonly used for dose-averaged LET (LETd) calculations,[6–8] Most of these kernel approaches, although keep accuracy in central axis calculations, are not able to describe accurately the lateral profile observed when calculating LETd in proton beams using MC. More generally, pencil beam algorithms are not as accurate as Monte Carlo (MC) techniques, which can be considered as the gold standard,[6] especially when dealing with inhomogeneities.[7–9] These shortcomings of the kernel based models makes necessary to add ad-hoc corrections or to use more complex models.[9]

Pencil beam algorithms also require dedicated functions for each quantity to calculate, doubling the workload if both dose and LETd need to be determined. Again, MC methods are able to overcome this limitation since in a single simulation it is possible to score several quantities in a volume of interest. However, the computation requirements for MC simulations in terms of time and resources are clearly higher than for analytical algorithms.

In this work, a different approach is proposed to address calculations of different quantities of interest (QOIs) in proton therapy, and particularly, LETd. Instead of using specific

quantity-depending kernels (such as dose kernels or LET kernels), a more general kernel for the spectrum of proton beams (in terms of kinetic energy or, equivalently, range of the particles) at each spatial point, that is, spectral fluence, is proposed. This allows for a more MC-alike approach since the information about the density of particles present and their energy is taken into account along their whole path. Then, simultaneous calculations for polyenergetic beams can be carried out by integrating the corresponding function on the energy for each QOI. Here, we present the particular results for LETd by using the stopping power data from NIST. Additionally, in previous works we have developed some functions dependent on the kinetic energy of protons to calculate dose-mean linear energy (y_D) and LETd from microdosimetry by using MC simulations.[10,11] The method presented here also enables calculations of three-dimensional distributions of these microdosimetric QOIs.

2. MATERIALS AND METHODS

2.A. General calculations of QOIs

Stopping power for protons and other particles is generally available in terms of the kinetic energy of the particle from different databases.[12,13] Such energy-dependent functions need the knowledge of the particle spectrum in order to be used. In this way, if $\phi(\boldsymbol{r})$ is the fluence at a point $\boldsymbol{r}$, given the spectral fluence $\phi_E(E;\boldsymbol{r}) \equiv \mathrm{d}\phi(\boldsymbol{r})/\mathrm{d}E$ at a certain point $\boldsymbol{r}$, the average value for a generic energy-dependent function $q = q(E)$ at that point will be given by

$$\overline{q}(\boldsymbol{r}) = \frac{\int q(E)\phi_E(E;\boldsymbol{r})\mathrm{d}E}{\int \phi_E(E;\boldsymbol{r})\mathrm{d}E} \tag{1}$$

Possible simple examples of quantities based on electronic stopping power $S(E)$ that can be calculated with Eq. (1) are: (i) dose, by introducing $q(E) = S(E)/(A\rho)$ in the integration, where A is the cross-sectional area of a voxel and ρ is the physical density of water; or (b) track-averaged LET, $\overline{L}_T$, by simply exchanging $q(E) = S(E)$. Furthermore, more complex quantities can be calculated as well, such as dose-averaged LET ($\overline{L}_D$), by computing separately Eq. (1) with $q(E) = S^2(E)$ and $q(E) = S(E)$ and dividing the final results. The latter example is used in this work to show results. Therefore, this work is centered on how to determine $\phi_E(E;\boldsymbol{r})$ as this quantity allows for a variety of different calculations of interest.

In Eq. (1), the spectral fluence $\phi_E(E)$ acts as a weight for each spectral component in the energy-dependent function $q(E)$. Equivalently, if the relation between energy and range in the continuous slow-down approximation (CSDA) is known, $R = R(E)$, then the average value for q at a point $\boldsymbol{r}$ can be alternatively computed as

$$\overline{q}(\boldsymbol{r}) = \frac{\int q(R)\phi_R(R;\boldsymbol{r})\mathrm{d}R}{\int \phi_R(R;\boldsymbol{r})\mathrm{d}R} \tag{2}$$

where $\phi_R(R;\boldsymbol{r}) \equiv \mathrm{d}\phi(\boldsymbol{r})/\mathrm{d}R$ is the fluence range-density, that is the relative number of particles per cross-sectional unit area with CSDA range equal to R with respect to the total number of particles per cross-sectional unit area at $\boldsymbol{r}$. This second approach is preferred because of practical reasons. Concretely, the variation of stopping power and other QOIs with the CSDA range is smoother than with the particle energy, assuming as this relation $R(E) = \alpha E^p$, that is, the Bragg-Kleeman rule.[14] Therefore, if the energy-dependent functions $\{q_j(E)\}$ and the transform rule to CSDA range $R = R(E)$ are known, according to Eq. (2), our problem is reduced to the determination of $\phi_R(R;\boldsymbol{r})$ at each point of interest.

2.B. Application to clinical beams

A clinical beam is generally composed of the superposition of several layers, being each one of them calculated independently. In a pencil beam scanning (PBS) system, a beam is composed of spots that are magnetically scanned to achieve a conformal dose distribution. Note that a layer is here defined by a nominal energy, a reference system (beam angle and isocenter position) and a two-dimensional map of spot-fluence weights. In this context, $\phi_R(R;\boldsymbol{r})$ is the total resulting fluence range-density and is obtained as a combination of the fluence range-density for each beam, which, in turn, is a combination of the individual fluence coming from each spot. Let N_L be the number of layers present in a given beam and $\phi_{R,i}(R;\boldsymbol{r})$ the fluence range-density for the i-th layer. If $\phi_i(\boldsymbol{r})$ is the total fluence that the i-th layer carries to the point $\boldsymbol{r}$, then

$$\phi_R(R;\boldsymbol{r}) = \frac{\sum_{i=1}^{N_L} \phi_i(\boldsymbol{r})\phi_{R,i}(R;\boldsymbol{r})}{\sum_{i=1}^{N_b} \phi_i(\boldsymbol{r})} \tag{3}$$

Equation (3) represents a weighted average for the different spectral fluence converging at a point $\boldsymbol{r}$, in which the weights are their corresponding fluences. Consequently, it becomes necessary to determine the number of particles per area unit carried by each layer at each point. This determination, however, is a problem frequently solved in pencil beam algorithms as follows. A treatment planning system (TPS) with pencil beam scanning (PBS) system, should provide the following information of a layer: (a) its nominal energy with a certain initial spread τ_{ini}; and (b) the lateral width of the spots $\sigma_{lat,spot}(z)$ on that layer at a certain reference depth, normally the isocenter.[15] In this sense, $\phi_{R,i}(\boldsymbol{r})$ can be obtained by summing the contributions from every individual spot composing it and, in turn, that contribution for each spot is obtained from the composition of different infinitely narrow beam, usually called beamlets. Then, it is convenient to separate the problem of determining $\phi_{beamlet}(\boldsymbol{r})$ for each beamlet into two different functions: one depending only on the depth

in water (integrated fluence, that is, total number of particles at each depth) and the other depending on the lateral distance to the beam propagation axis ρ at each depth z, $\phi_{beamlet}(\boldsymbol{r}) = (\Phi_{int}(z)/\Phi_0)\phi_{lat,beamlet}(\rho;z)$, where $\Phi_{int}(z)/\Phi_0$ represents the fraction of particles arriving at each depth with respect to the total number of particles coming from the water surface.

Now, $\sigma_{lat,spot}(z)$ refers to the width of the spot's lateral profile for the fluence at a depth z for a layer, which becomes larger as it goes away from the source due to the beam divergence. Furthermore, when those particles travel through matter (particularly, water), they undergo scattering processes thus the lateral distribution of particles becomes broader. This can be incorporated by generating a lateral kernel for a beamlet, which, essentially, represents the probability density for a particle to reach each lateral position. In other words, if at a certain depth z the probability density for a single particle to be scattered up to a lateral distance ρ is given by $K_w(\rho;z) = \phi_{lat,beamlet}(\rho;z)$, then the fluence for a spot at that point will be given by the convolution.

$$\phi_{spot}(\boldsymbol{r}) = \frac{\Phi_{int}(z)}{\Phi_0}\int \phi_{lat,spot}(\rho';z)K_w(\rho'-\rho;z)d\rho' \qquad (4)$$

here, again, $\phi_{lat,spot}(\rho;z)$ represents the fluence for each spot coming from the nozzle taking into account the beam divergence and it is usually provided by the TPS and modeled as a single Gaussian function thus $\phi_{lat,spot}(\rho;z) = \exp\left(-\rho^2/\left(2\sigma^2_{lat,spot}(z)\right)\right)$. Finally, the fluence for the overall i-th layer is obtained by convolving again the fluence for a single spot at each depth, $\phi_{spot}(\boldsymbol{r})$, with its two-dimensional map of spot weights produced by the PBS system, $w(x,y)$:

$$\phi_i(\boldsymbol{r}) = \int \phi_{spot}(x',y';z)w(x-x',y-y')dx'dy' \qquad (5)$$

where now lateral coordinates have been transformed from cylindrical to Cartesian. This way Eq. (5) provides the weights in the weighted average of spectral fluences shown in Eq. (3).

2.C. Beam components

Generally, we can distinguish between two different types of particle components present in a beam according to their different behavior in depth and laterally. In this work, we use the distinction provided by the MC package Geant4[16–18]: primary particles are those that have undergone only electromagnetic and hadronic elastic collisions while secondary particles are those generated in nuclear inelastic collisions and in charge-exchange processes. Furthermore, we can differentiate between secondary particles with equal or different nature than the primaries, for example, in a proton beam, we have three categories: primary protons, secondary protons, and the rest of secondary particles. Each one of these categories contains particles with diverse behavior. In other words, the functions $\Phi_{CAX,P}(z)$ and $K_{w,P}(\rho;z)$ vary depending on the type of particle P considered. Additionally, the fluence range-density $\phi_{R,i}(R;\boldsymbol{r})$ also depends on the type of particle so that each category needs to be considered separately up to Eq. (3). Then, Eq. (2) becomes

$$\overline{q}(\boldsymbol{r}) = \frac{\int \sum_{P=1}^{N_P} q_P(R)\phi_{R,P}(R;\boldsymbol{r})\mathrm{d}R}{\int \sum_{P=1}^{N_P} \phi_{R,P}(R;\boldsymbol{r})\mathrm{d}R} \qquad (6)$$

where N_P is the number of types of particles and $q_P(R)$ and $\phi_{R,P}(R;\boldsymbol{r})$ are, respectively, the function of interest and the outcome of Eq. (2) for the type of particle P.

2.D. Models for proton beams: Monte Carlo simulations

As said, a new methodology is here proposed, somehow similar to a conventional pencil beam algorithm. However, pencil beam algorithms traditionally model the dose (or LET) deposited by a beamlet (i.e. a kernel). Then, the total dose for a broad beam is computed by convolving the kernel across the plurality of beamlets that a beam is composed of. It is important to remark that we do not use dose- or LET-based kernels, but fluence (i.e., number of particles per area unit, which is closely related to dose) and, particularly, spectral fluence (i.e., distribution of energy of the particles in a beamlet). To our knowledge, while the majority of the functions used here to model the fluence kernel are common from pencil beam algorithms, the proposed kernels and procedures for obtaining spectral fluence are new.

According to all above, in order to end up obtaining the value $q(\boldsymbol{r})$ we need to determine the functions $\phi_{R,P}(R;\boldsymbol{r})$, $\Phi_{int,P}(z)$ and $K_{w,P}(\rho;z)$ for all the components of the beam to be considered. We have developed analytical forms for these functions applied to the case of proton beams with energies in the typical clinical range: from 50 to 250 MeV at intervals of 25 MeV. MC simulations for the transport of $5\cdot10^7$ protons in liquid water have been performed with Geant4 v10.5.0 for each one of these energies; QGSP_BIC_HP with the most accurate physics list, G4EmStandardPhysics option4, was used. Three types of particles are distinguished: primary protons, secondary protons and secondary alpha particles. So far, the rest of particles generated in such interactions are disregarded in this model due to their low proportion[19] for the sake of simplicity and efficiency.

It is worth to note that, apart from the explicit dependencies already shown, the functions to model also depend on the nominal energy of the layer under consideration, E_0, therefore this dependency is introduced explicitly as well. As seen in Eq. (4), the function $K_{w,P}(\rho;z;E_0)$ needs first to be convolved with $\Phi_{lat,spot}$, which is usually a Gaussian function given by the TPS, and later with the spot weights map $w(x,y)$, as shown in Eq. (5). As the convolution operation between Gaussian functions becomes as easy as a quadratic sum of the σ parameters, we look for single or multiple Gaussians to model $K_{w,P}(\rho;z;E_0)$ by fitting these functions to the lateral distributions obtained from our MC simulations. For

the depth dependency no special operations are needed so that $\Phi_{int,P}(z;E_0)$ is open to any functional form able to produce good agreement with MC data. Finally, $\phi_{R,P}(R;\boldsymbol{r})$ can be modeled as any well-behaved function to perform the integrations in Eq. (6).

2.D.1. Number of particles with depth in water

The dependency of the number of primary protons (*PP*) at each depth can be modeled, according to Ulmer's work,[4] by a function as the following one:

$$\frac{\Phi_{int,PP}(z;E_0)}{\Phi_0(E_0)} = \left(1-\frac{\xi(E_0)z}{R(E_0)}\right)\frac{1}{2}\left(1+\mathrm{erf}\left(\frac{R(E_0)-z}{\sqrt{2}\tau(E_0)}\right)\right) \tag{7}$$

where $\Phi_0(E_0)$ is the number of protons reaching the water surface ($z=0$), $R(E_0)$ is the CSDA range of protons with energy E_0 and $\xi(E_0)$ and $\tau(E_0)$ are the parameters of the model. The dependency on the nominal energy of the layer is addressed as follows: the function proposed in Eq. (7) is fitted against the results from MC simulations for each one of the simulated energies. Therefore, a set of values for the parameters $\xi(E_0)$ and $\tau(E_0)$ are obtained. To calculate the function $\Phi_{int,PP}(z;E_0)$ for an energy E_0' between two simulated energies, we first define the depth-scaled to the range $z_{sc}(E_0)=z/R(E_0)$. Then, $\Phi_{int,PP}\left(z_{sc}^{\uparrow};E_0^{\uparrow}\right)$ and $\Phi_{int,PP}\left(z_{sc}^{\downarrow};E_0^{\downarrow}\right)$ are computed according to Eq. (6), where $E_0^{\uparrow}$ and $E_0^{\downarrow}$ are, respectively, the immediately higher and lower simulated energies to E_0' and $z_{sc}^{\uparrow}$ and $z_{sc}^{\downarrow}$ are the depth-scaled to the range corresponding to those energies. Finally, a linear interpolation between those two values is performed so that

$$\begin{aligned}\Phi_{int,PP}\left(z;E_0'\right) &= \Phi_{int,PP}\left(z_{sc}^{\downarrow};E_0^{\downarrow}\right)\\ &+\left(\Phi_{int,PP}\left(z_{sc}^{\uparrow};E_0^{\uparrow}\right)-\Phi_{int,PP}\left(z_{sc}^{\downarrow};E_0^{\downarrow}\right)\right)\frac{E_0'-E_0^{\downarrow}}{E_0^{\uparrow}-E_0^{\downarrow}}\end{aligned} \tag{8}$$

This is the approach followed to compute all the functions here presented for any nominal energy between the simulated ones.

For the number of secondary protons (*SP*) at each depth, we propose the function:

$$\begin{aligned}\frac{\Phi_{int,SP}(z;E_0)}{\Phi(E_0)} = \frac{\xi(E_0)z}{R(E_0)}\frac{1}{2}\left(1+\mathrm{erf}\left(\frac{R(E_0)-z}{\sqrt{2}\tau(E_0)}\right)\right)\\ \left(\alpha_0(E_0)-\alpha_1(E_0)z^{\alpha_2(E_0)}\right)\end{aligned} \tag{9}$$

where $\Phi_0(E_0)$, $R(E_0)$, $\xi(E_0)$ and $\tau(E_0)$ are the same as in Eq. (7) and $\alpha_0(E_0)$, $\alpha_1(E_0)$ and $\alpha_2(E_0)$ are the parameters to be determined. These parameters have no physical meaning since the function has been selected to achieve a good fit to the MC results.

We also propose a similar function to model the proportion of alpha particles (AP) in depth:

$$\frac{\Phi_{int,AP}(z;E_0)}{\Phi_0(E_0)} = P_4(z;E_0)\left(1+\mathrm{erf}\left(\frac{R(E_0)-z}{\sqrt{2}\tau_{AP}(E_0)}\right)\right) \tag{10}$$

where $\Phi_0(E_0)$ and $R(E_0)$ are the same as in Eq. (7), $\tau_{AP}(E_0)$ is a parameter and $P_4(z;E_0)$ is a fourth-grade polynomial function that carries five additional parameters for each simulated energy.

2.D.2. Lateral kernel

Lateral kernels for fluence are similar to other pencil beam algorithms use for dose. Here, The lateral kernel $K_{w,PP}(\rho;z;E_0)$ for the fluence of primary protons is modeled simply as a single Gaussian centered at the central axis and normalized:

$$K_{w,PP}(\rho;z;E_0) = \frac{1}{\sqrt{2\pi}\sigma_{lat,PP}(z;E_0)}\exp\left(-\frac{\rho^2}{2\sigma_{lat,PP}^2(z;E_0)}\right) \tag{11}$$

The parameter $\sigma_{lat,PP}(z;E_0)$ is enough to characterize the function although its dependency on depth needs to be determined. In order to do that, for each simulated nominal energy E_0, we fit $K_{w,PP}(\rho;z;E_0)$ to the obtained lateral distributions at each depth z with intervals of 0.5 mm and obtain $\sigma_{lat,PP}(z;E_0)$. The dependency of this parameter with depth is modeled, for each nominal energy E_N, as a polynomial function:

$$\begin{aligned}\sigma_{lat,PP}(z;E_0) = a_{0,PP}(E_0)+a_{1,PP}(E_0)z+a_{2,PP}(E_0)z^2\\ +a_{3,PP}(E_0)z^3\end{aligned} \tag{12}$$

Lateral distributions for secondary protons have a more prominent tale than for primaries, so that a second Gaussian is needed for a better fit to the MC results. Therefore, we have

$$\begin{aligned}K_{w,SP} = \frac{w_{SP}(z;E_0)}{\sqrt{2\pi}\sigma_{l1,SP}(z;E_0)}\exp\left(-\frac{\rho^2}{2\sigma_{l1,SP}^2(z;E_0)}\right)\\ +\frac{(1-w_{SP}(z;E_0))}{\sqrt{2\pi}\sigma_{l2,SP}(z;E_0)}\exp\left(-\frac{\rho^2}{2\sigma_{l2,SP}^2(z;E_0)}\right)\end{aligned} \tag{13}$$

where now three parameters are needed to characterize the kernel: $w_{SP}(z;E_0)$, $\sigma_{l1,SP}(z;E_0)$ and $\sigma_{l2,SP}(z;E_0)$. These parameters are obtained for each depth according to polynomial functions of first, second and third-grade, respectively, similar to the one in Eq. (12).

For the lateral distribution of alpha particles fluence, a single Gaussian can be used so that

$$K_{w,AP}(\rho;z;E_0) = \frac{1}{\sqrt{2\pi}\sigma_{lat,AP}(z;E_0)}\exp\left(-\frac{\rho^2}{2\sigma_{lat,AP}^2(z;E_0)}\right) \tag{14}$$

where $\sigma_{lat,AP}(z;E_0)$ is obtained as a function of depth by fitting a third-grade polynomial function, as in the case of primary protons shown in Eq. (12).

2.D.3. Fluence range-density or spectrum in terms of CSDA range

While the previous functions are intended to provide fluences similarly as done in other pencil beam algorithms, our formalism differs when characterizing the kernels for beamlets' spectra. In order to determine the spectral components of the beam at each point, here $\phi_{R,P}(R;\boldsymbol{r};E_0)$ represents the probability density for the CSDA range at each spatial position when a single particle of energy E_0 is considered. For all types of particles here presented, $\phi_{R,P}(R;\boldsymbol{r};E_0)$ is modeled as a single normalized Gaussian function, which is fully characterized by two parameters: mean $\mu_{R,P}(\boldsymbol{r};E_0)$ and standard deviation $\sigma_{R,P}(\boldsymbol{r};E_0)$. This means that, at each point $\boldsymbol{r}$, the probability density for a particle of type P and initial energy E_0 corresponding to a given CSDA range is given by

$$\phi_{R,P}(R;\boldsymbol{r};E_0)=\frac{1}{\sqrt{2\pi}\sigma_{R,P}(\boldsymbol{r};E_0)}\exp\left(-\frac{\left(R-\mu_{R,P}(\boldsymbol{r};E_0)\right)^2}{\sigma^2_{R,P}(\boldsymbol{r};E_0)}\right) \tag{15}$$

when a particle penetrates in water, its probability to appear at a certain point decreases with the distance from the central axis. In the same way, the particle energy spectrum also depends on the position. Concretely, in a central axis point, the particle likely will have a higher energy than in a radial point. In other words, the mean of $\phi_{R,P}(R;\boldsymbol{r};E_0)$ decreases radially. We can use, in a similar way than for the fluence, a decomposition in terms of depth and lateral components thus

$$\mu_{R,P}(\boldsymbol{r};E_0)=\mu_{CAX,P}(z;E_0)K_{\mu_{R,P}}(\rho;z;E_0) \tag{16}$$

where $K_{\mu_{R,P}}(\rho;z;E_0)=\exp\left(-\rho^2/2\sigma^2_{lat,\mu_{R,P}}(z;E_0)\right)$ is taken again as a Gaussian function on the radial position to the central axis, as in Eq. (11) and represents the lateral variation for the mean CSDA range $\mu_{R,P}(\boldsymbol{r};E_0)$. The dependency of parameters $\mu_{CAX,P}(z;E_0)$ and $\sigma_{lat,\mu_{R,P}}(z;E_0)$ with depth is modeled again by polynomial functions. An exception is the case of primary protons, in which the mean of the spectrum in terms of CSDA range is taken as the residual range, that is, $\mu_{CAX,P}(z;E_0)=R(E_0)-z$. Note that $K_{\mu_{R,P}}(\rho;z;E_0)$ is, by itself, a new lateral kernel, so that the actual mean value $\mu_{R,P}(\boldsymbol{r};E_0)$ at a point $\boldsymbol{r}$ for a spot with lateral fluence in air $\Phi_{lat,spot}(\rho;z)$ is given by a new convolution:

$$\mu^{spot}_{R,P}(\boldsymbol{r};E_0)=\mu_{CAX,P}(z;E_0)\int\Phi_{lat,spot}(\rho';z)K_{w,P}(\rho'-\rho;z)K_{\mu_{R,P}}(\rho'-\rho;z;E_0)d\rho' \tag{17}$$

where we have excluded the explicit energy dependency for simplification. Note that the mean $\mu_{R,P}(\boldsymbol{r};E_0)$ needs to be obtained by convolving the model for single particles, given in Eq. (16), with the actual number of particles coming from

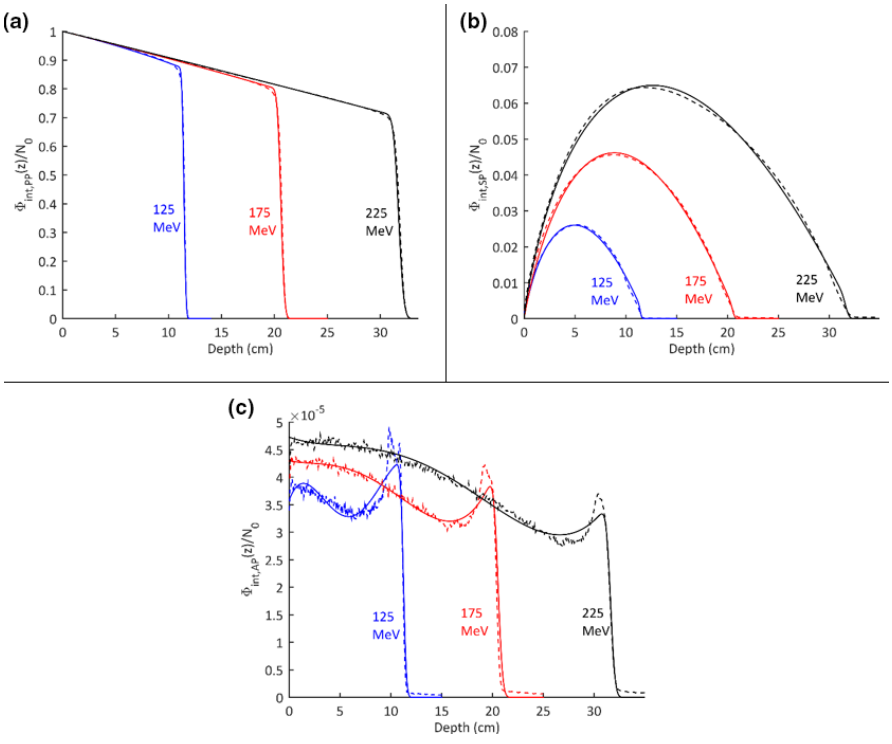

FIG. 1. Fraction of (a) primary protons, (b) secondary protons and (c) alpha particles in depth respect to the number of protons arriving at water surface (N_0). Dashed lines represent the results obtained from Geant4 simulations for protons of 125 MeV (blue), 175 MeV (red) and 225 MeV (black). Solid lines are the fits obtained with the functions shown in Eqs. (7), (9) and (10) for the panels (a), (b) and (c), respectively. (a) - — Geant4 simulation; —— Eq. (7). (b) - — Geant4 simulation; —— Eq. (9). (c) - — Geant4 simulation; —— Eq. (10). [Color figure can be viewed at wileyonlinelibrary.com]

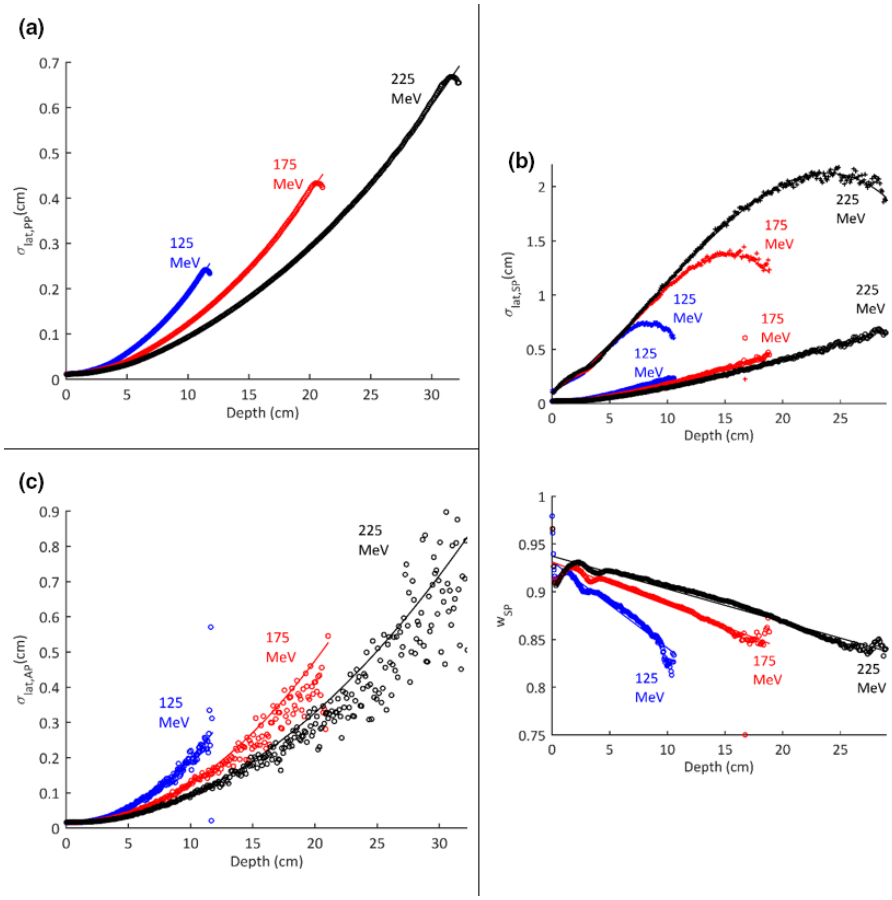

FIG. 2. Parameters to characterize the lateral distribution for (a) primary protons, (b) secondary protons and (c) alpha particles for three different energies: 125 MeV (blue), 175 MeV (red) and 225 MeV (black). Polynomial functions are fitted to the points, obtained, in turn, by fitting a single Gaussian functions in the cases (a) and (c) and Double Gaussian functions for the case (b) to the lateral profile at each independent depth. These parameters correspond to those in Eqs. (11), (13) and (14) and are used to build the lateral kernels at each depth and for each energy. (a) ○ $\sigma_{lat,PP}$ obtained from Single Gaussian fit to Geant4 data; ── Polynomial fit; Equation (11). (b) ○ $\sigma_{l1,SP}$ and w_{SP} obtained from Double Gaussians fits to Geant4 data; + $\sigma_{l2,SP}$ obtained from Double Gaussians fits to Geant4 data; ── Polynomial fits. (c) ○ $\sigma_{lat,AP}$ obtained from Single Gaussian fit to MC data; ── Polynomial fit. [Color figure can be viewed at wileyonlinelibrary.com]

the spot, which includes the lateral fluence kernel $K_w(\rho;z)$ as shown in Eq. (4). Again, the mean value at each point for the overall layer is obtained by convolving Eq. (16) with the spot weights map:

$$\mu_{R,P}(\boldsymbol{r};E_0) = \int \mu_{R,P}^{spot}(x',y',z;E_0)w(x-x',y-y')dx'dy' \tag{18}$$

In contrast with the mean value, in order to reduce the complexity of the model, standard deviation is considered as constant laterally, i.e. $\sigma_{R,P}(\boldsymbol{r};E_0) = \sigma_{R,P}(z;E_0)$. This parameter, again, is modeled in depth as a polynomial function.

2.E. Application to a particular quantity: Dose-averaged LET calculation

Let us consider the case of calculating dose-averaged LET using the fluence kernel proposed above. Dose-average LET is defined as[20]

$$\overline{L}_D(\boldsymbol{r}) = \frac{\int S^2(E)\phi_E(E;\boldsymbol{r})dE}{\int S(E)\phi_E(E;\boldsymbol{r})dE} = \frac{\overline{S^2}(\boldsymbol{r})}{\overline{S}(\boldsymbol{r})} \tag{19}$$

where $S(E)$ is the electronic stopping power of the considered particle as a function of its kinetic energy. This can be calculated according to Eq. (5) at each point $\boldsymbol{r}$ as,

$$\overline{S^2}(\boldsymbol{r}) = \frac{\int \sum_{P=1}^{N_P} S_P^2(R)\phi_{R,P}(R;\boldsymbol{r})\mathrm{d}R}{\int \sum_{P=1}^{N_P} \phi_{R,P}(R;\boldsymbol{r})\mathrm{d}R} \tag{20}$$

and

$$\overline{S}(\boldsymbol{r}) = \frac{\int \sum_{P=1}^{N_P} S_P(R)\phi_{R,P}(R;\boldsymbol{r})\mathrm{d}R}{\int \sum_{P=1}^{N_P} \phi_{R,P}(R;\boldsymbol{r})\mathrm{d}R} \tag{21}$$

where all symbols coincide with those in Eq. (6) exchanging the generic quantity $q_P(R)$ by $S_P^2(R)$ and $S_P(R)$, respectively. Note that now the stopping power $S_P(R)$ for the particle P is expressed in terms of the CSDA range instead of the energy of the particle. It is possible to perform such integrations by using the model presented in the previous section and the

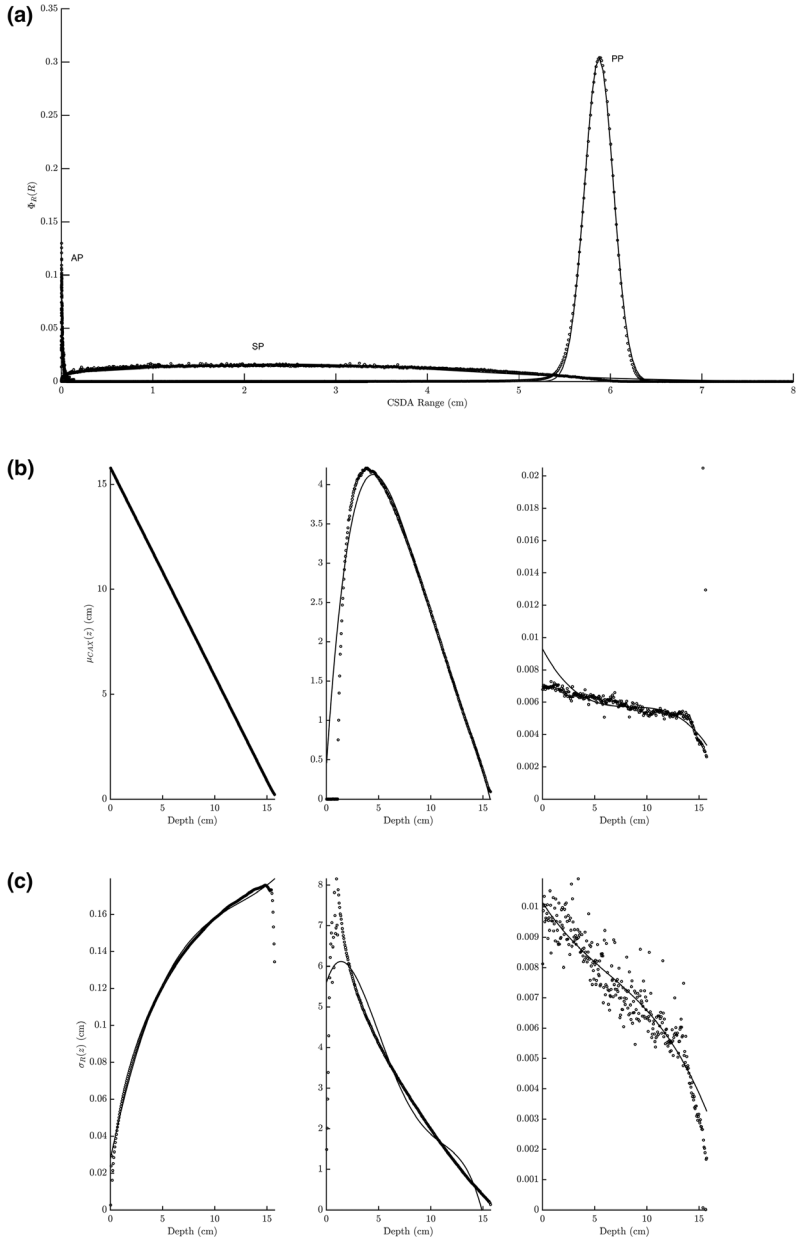

FIG. 3. (a) Examples of spectra for primary protons, secondary protons and alpha particles in terms of continuous slow-down approximation range for a single-layer proton beam of 150 MeV at a depth equal to 10 cm. (b) Mean of the spectra shown in (a) in depth for each type of particle for a single-layer proton beam of 150 MeV. For primary protons (left), this is modeled as the residual range, whereas for secondary protons (middle) and alpha particles (right) a third-grade polynomial function is used. (c) Standard deviation of the spectra shown in (a) considered as a Gaussian function for a single-layer proton beam of 150 MeV for primary protons (left), secondary protons (middle) and alpha particles (right). (a) ○ Geant4 simulations; —— Single Gaussian fits. (b) ○ Mean $\mu_{R,P}$ of the Gaussian function fitted to Geant4 simulations; ——Polynomial fits. (c) ○ Sigma $\sigma_{R,P}$ of the Gaussian function fitted to Geant4 simulations; —— Polynomial fits.

stopping power and range data for each energy in the NIST databases.[12]

This model has been implemented in C# code and integrated into the Varian Eclipse TPS (version 15) through the Eclipse Scripting Application Programming Interface (ESAPI)[21] in order to calculate three-dimensional (3D) distributions in real clinical proton beams. All calculations were performed with a beam model of a pencil beam scanning (PBS) system from IBA. A parallelepiped structure with 10 cm in-length and square base (5.5 cm × 5.5 cm) is defined in a large cube of liquid water with its distal face at 20 cm in-depth. A beam is generated in Eclipse to produce a uniform dose over that structure. To benchmark the results, the same geometry is simulated using the fast MC code MCsquare[22] by simulating 10^9 primary particles. The LETd calculations are computed in MCsquare by using the scoring method labeled as "C" in Cortes-Giraldo and Carabe's work.[23] We performed two comparisons: (a) only considering primary and secondary protons in both systems and (b) adding just the alpha particles'

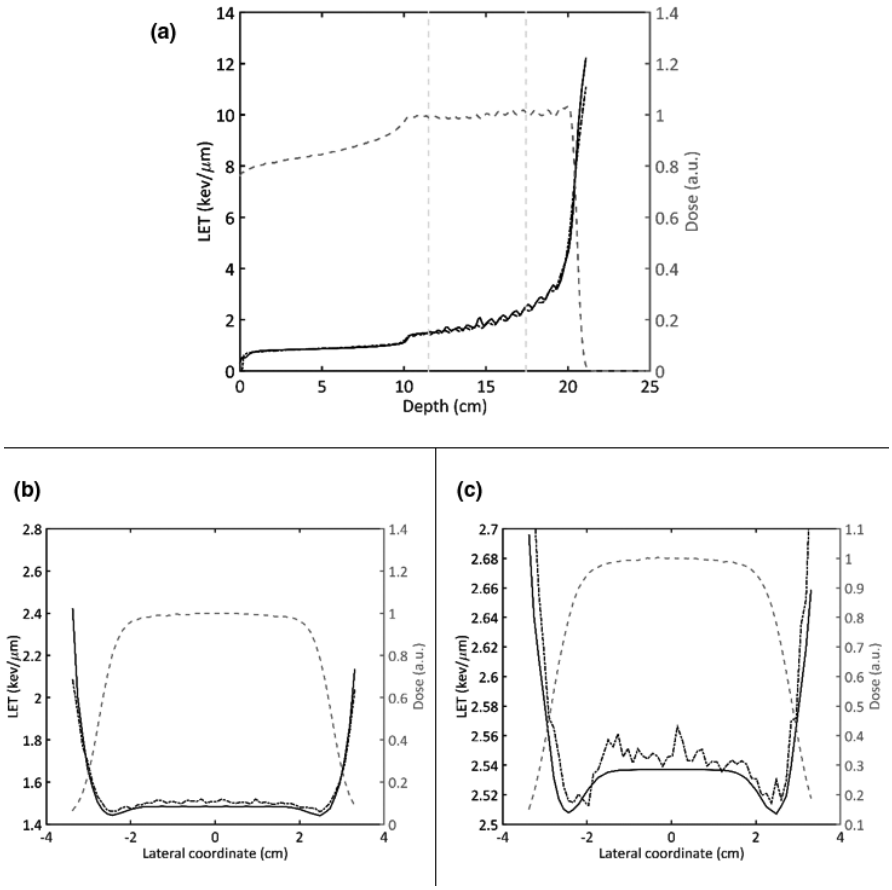

FIG. 4. Calculations of LETd considering only protons with our fluence kernel-based method and with MCsquare (10^9 protons simulated) for a spread-out Bragg peak with maximum range of 20 and 10 cm of modulation at (a) the central axis, (b) a lateral profile at depth = 11.5 cm and (c) another lateral profile at depth = 17.44 cm. The positions of the lateral profiles are marked in (a) with gray vertical lines. Dose calculations with MCsquare are shown in gray dashed lines. —— Fluence kernel-based calculation; - — - MCsquare.

contribution in our method and in MCsquare, with a specially devoted version for this work.

Finally, we also have performed calculations in medium different from water. In order to do that, the depth in water, z, is replaced by the corresponding water-equivalent thickness z_{WET} resulting from the beam raytracing throughout all the previous equations. We consider a prostate case treated with two single-field-optimized lateral beams and compare the distributions of $\overline{L}_D$ resulting from our method and MCsquare.

3. RESULTS

Figure 1 shows the integrated fluence at each depth for primary protons, secondary protons and alpha particles obtained from simulations with Geant4. Fits for the functions shown in Eqs. (7), (9) and (10) are also shown. Results for only three energies (125, 175, and 225 MeV) are shown to ease the visualization. Similar trends are obtained for the rest of the energies. As a measurement of the goodness of the fits, for primary protons the nine simulated energies provide a mean $R^2 = 0.998$, for secondary protons $R^2 = 0.995$ and for alpha particles $R^2 = 0.986$.

Lateral distributions for primary protons and secondary alphas are modeled as single Gaussian functions at every individual depth considered. Whereas, for secondary protons, a double Gaussian function is employed. The goodness of these fits can be evaluated through the mean R^2 for each one of the nine energies employed. The averages and standard deviations of these sets of nine mean R^2 are 0.997 ± 0.0004 for primary protons, 0.982 ± 0.0007 for secondary protons and 0.993 ± 0.003 for alpha particles. Figure 2 shows the dependency of the lateral σ for each case for the same three selected energies than in Fig. 1.

The spectrum in terms of CSDA range for each component is modeled as a single Gaussian function. Figure 3(a) shows an example of the spectrum obtained from Geant4 MC simulations and the fitted functions (beam energy of 150 MeV at 10 cm in depth). The overall goodness of this fits is evaluated through the average of the mean R^2 parameters obtained for each energy along all the considered depths: 0.995 ± 0.001 for primary protons, 0.938 ± 0.025 for secondary protons and 0.90 ± 0.02 for alpha particles. Figure 3(b) shows the dependency of the mean range on the depth for the same beam energies. Note that the relation between CSDA range and kinetic energy is different for

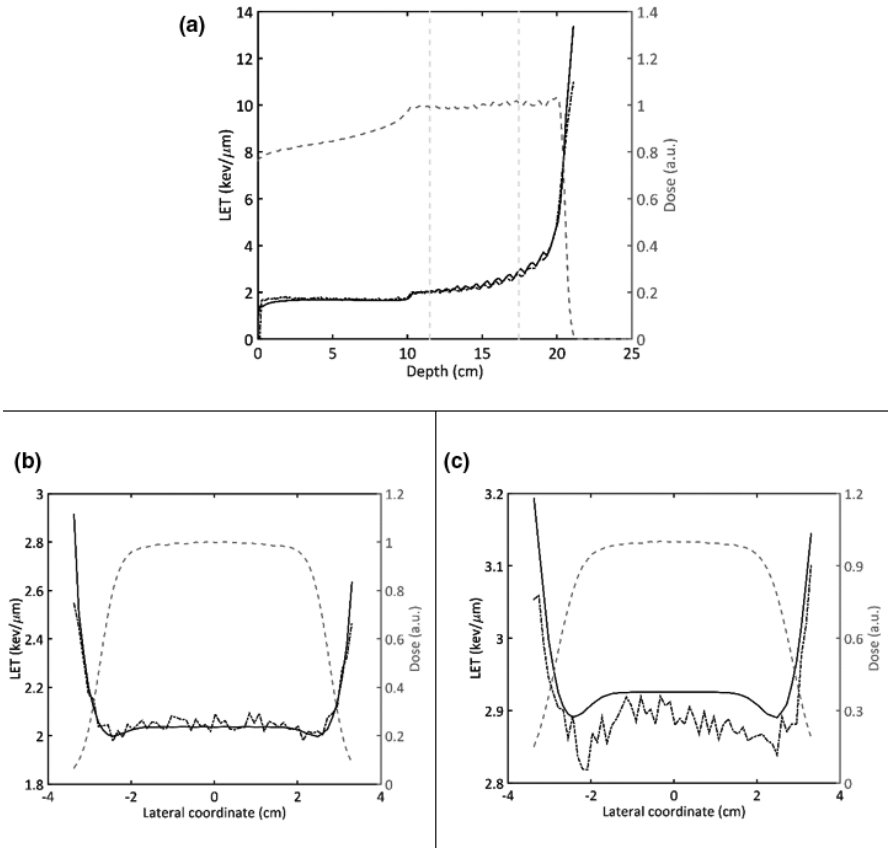

FIG. 5. Calculations of LETd considering protons and alpha particles with our fluence kernel-based method and a specially compiled version of MCsquare that includes only primary protons, secondary protons and secondary alpha particles (10^9 primary particles simulated) for a spread-out Bragg peak with maximum range of 20 and 10 cm of modulation at (a) the central axis, (b) a lateral profile at depth = 11.5 cm and (c) another lateral profile at depth = 17.44 cm. The positions of the lateral profiles are marked in (a) with gray vertical lines. Dose calculations with MCsquare are shown in gray dashed lines. —— Fluence kernel-based calculation; - — - MCsquare.

protons and for alpha particles. Figure 3(c) shows the standard deviation for the Gaussian functions for the same beam than in Figs. 3(a) and 3(b).

Figure 4 shows the comparison between the calculations for LETd by using the fluence kernel method exposed in this work and by MCsquare only considering primary and secondary protons. Results at the central axis are shown in Fig. 4(a) whereas Figs. 4(b) and 4(c) show two lateral profiles at different depths. The mean difference between two results along the central axis, taking samples separated by 1 mm, is -0.29 ± 0.15 keV/μm, where uncertainty is expressed as one standard deviation of the mean difference. For the whole three-dimensional distribution, we find a mean difference of -0.007 ± 0.008 keV/μm. Points with a number of particles less than 1% of the total number of particles coming for each layer are excluded from this computation.

The same case but adding the alpha particles' contribution to the fluence kernel and all the secondary heavier particles in MCsquare is shown in Fig. 5. In this case, the mean deviation at the central axis is found as -0.24 ± 0.14 keV/μm, meanwhile for the complete distribution it now goes to -0.022 ± 0.007 keV/μm.

Results of the calculations for $\overline{L}_D$ in a prostate case are shown in Fig. 6. Besides the $\overline{L}_D$ distributions calculated with MCsquare and our method and their differences, dose distribution obtained with MCsquare is also provided to contrast areas in which $\overline{L}_D$ may result high but dose is very low. Mean difference between MCsquare and our method in all the volume irradiated above 5% of the dose is equal to 0.28 keV $\pm$ 0.23 keV/μm. However, for the voxels contained in the PTV, this mean difference decreases to 0.07 ± 0.11 keV/μm. In the rectum, in turn, mean difference is 0.0 ± 0.8 keV/μm.

4. DISCUSSION

Results for LETd calculation show a good performance of our fluence model, especially when only protons are considered (see Fig. 4), in which not only central axis profiles tend to coincide but also the characteristic lateral curvature is met at any depth. We have chosen specifically LETd to assess our method for two reasons: (a) the values for the stopping power are extensively validated and (b) it is a quantity strongly dependent on the spectrum and the relative number of particles from each category rather than on the overall number of particles, which would be the case of quantities as energy or dose absorbed. Because of that dependency, every part of the method needs to be

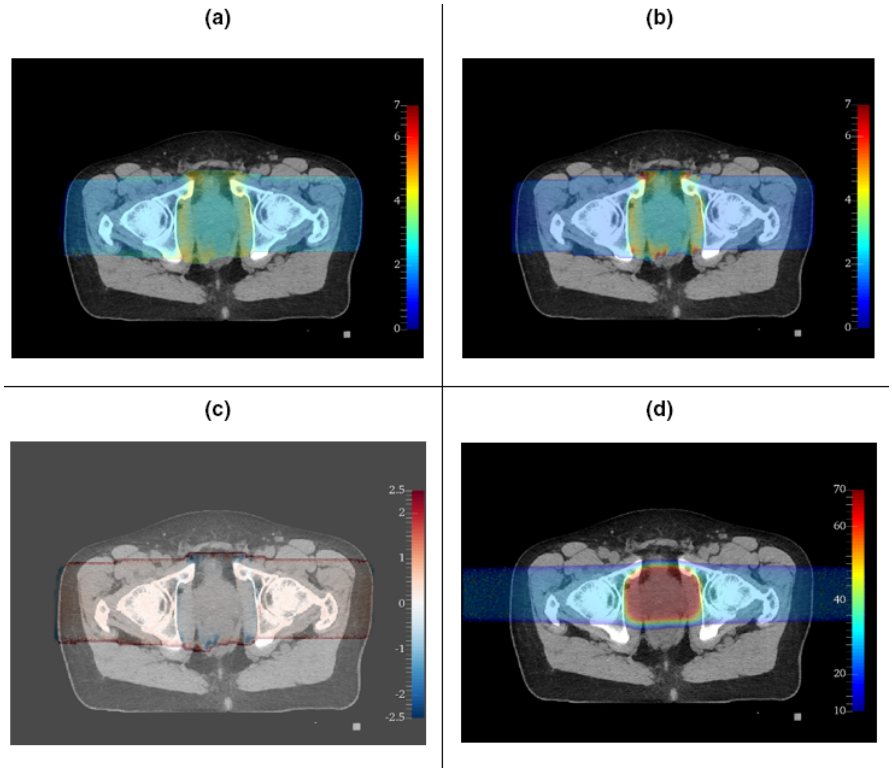

FIG. 6. Calculations on a central axial plane for prostate case with two lateral beams and a prescribed dose of 70.2 Gy. (a) $\overline{L}_D$ calculated with MCsquare. (b) $\overline{L}_D$ calculated with our method. (c) Difference between $\overline{L}_D$ calculated with MCsquare and with our method. (d) Dose distribution calculated with MCsquare. For (a), (b) and (c), color bars are specified in keV/μm. For (d), values on the color bar indicate Gy. [Color figure can be viewed at wileyonlinelibrary.com]

correctly modeled so that acceptable agreements with MC calculations can be found.

Even though our methodology uses convolution-superposition principles, as pencil beam algorithms do, the main difference here resides in the quantities to be superposed. While dose or LETd-specific kernels directly convolve and superpose curves of those quantities, we sum, on the one hand, the number of particles produced by each beamlet in a spot, and average, on the other hand, the mean energy of the particles traveling in that beamlet. These quantities can naturally be superposed under any condition whereas for dose, some assumptions need to be done: the energy deposition needs to be concentrated close around the particle track. The case of LETd is even worse: the non-linear component on the squared stopping power cannot be superposed in this way and artificial workarounds need to be incorporated to the lateral kernels.

However, some major deviations from the fluence data computed by Geant4 are observed in some cases. This is especially the case for the number of alpha particles in depth, as seen in Fig. 1(c), in which Eq. (9) appreciably deviates from the curve obtained from Geant4 around the end of the beam range. Nonetheless, the impact of these deviations is reduced since, as protons' stopping power increases in that area, the relative contribution to the LETd of alpha particles becomes small. Our models for secondary protons do not seem accurate at the entrance region [see Fig. 2(b) and Figs. 3(b) and 3(c)]. This can be explained by the small number of secondary protons produced there [see Fig. 1(b)], which makes unstable the Gaussian fits and, in turn, makes the values erratic for the parameters. Yet, precisely due to its relatively small number, the weight of these deviations in the calculations is limited. Finally, the relatively low R^2 values for the fits of Gaussian functions to the alpha particles are acceptable as a compromise for a simple meaningful function with few parameters, with the mean allowed to vary laterally.

We have included alpha particles in our formalism as they represent the main secondary contributor, besides protons, in clinical proton beams. Deuterons, for example, contributes to dose deposition by <0.1%, roughly an order of magnitude less than alpha.[19] However, deuterons and other particles might be incorporated following the same methodology to develop kernels for their fluence and spectral fluence. The contribution of alpha particles makes LETd increase especially at the entrance region, although our method seems to slightly underestimate this compared to MCsquare (see Fig. 5). However, the general agreement is remarkable and the entrance area is not expected to be particularly relevant to assess biological effect since LETd is relatively low there. In any case, as shown with alpha particles as an example, the contribution of any other particle can be added to the model by following a similar process: (a) obtaining the 3D distributions (number of particles and energy spectrum) for production of that particle in proton beams of a range of energies;

(b) model the functions for the number of particles in depth and laterally; and (ci) model the functions for the spectrum at the central axis and laterally.

It is important to remark that the method to consider inhomogeneous media here presented is a simple displacement of the calculated fluence according to the water-equivalent depth. This may result in errors for the lateral contribution of each beamlet to an adjacent point, especially around edges between two media highly inhomogeneous. Therefore, a more sophisticated method to overcome these situations is desirable. However, as shown in Fig. 6, average differences in $\overline{L}_D$ calculation as a surrogate of spectral fluence do not tend to be high, especially in areas in which dose, that is, fluence, is large.

Only LETd calculations are shown in this work as an example of the potential of this method. It should be noted, though, that an advantage here is the ability to simultaneously calculate a number of QOIs. For instance, if a function for the dependency of the dose on the energy of a particle, $D = D(E)$, can be found, then the same framework can be used to compute dose and LETd, which may lead to an efficient optimization process based on distributions of both quantities. Additionally, as mentioned before, our published microdosimetric functions[11] can be employed in order to generate three-dimensional distributions for them in commercial TPS.

5. CONCLUSIONS

A new analytical method to reproduce the three-dimensional distributions of spectral fluence in particle therapy is presented and particularized for the proton therapy case. The advantage of this spectral fluence-based approach is that several quantities of interest can be derived from the spectral fluence by means of a convolution integral as long as the dependency of those with the energy of the involved particles is known. As a specific application, LETd results with this approach look remarkably good even though only protons and alpha particles are taken into consideration. The philosophy of the method includes the potential of extending the considered particles by following a process similar to presented here.

ACKNOWLEDGMENTS

M. A. Cortés-Giraldo has been funded by the Spanish Ministry of Economy and Competitiveness under Grant No. FPA2016-77689-C2-1-R.

CONFLICT OF INTEREST

We would like to thank the associate editor for their valuables suggestions in order to improve this work. This project is supported by Varian Medical Systems, Palo Alto, California.

[a]Author to whom correspondence should be addressed. Electronic mail: a.carabe@pennmedicine.upenn.edu, alexcarabe@gmail.com.

REFERENCES

1. Hong L, Goitein M, Bucciolini M, et al. A pencil beam algorithm for proton dose calculations. *Phys Med Biol*. 1996;41:1305–1330.
2. Soukup M, Fippel M, Alber M. A pencil beam algorithm for intensity modulated proton therapy derived from Monte Carlo simulations. *Phys Med Biol*. 2005;50:5089–5104.
3. Pedroni E, Scheib S, Böhringer T, et al. Experimental characterization and physical modelling of the dose distribution of scanned proton pencil beams. *Phys Med Biol*. 2005;50:541–561.
4. Ulmer W. Theoretical aspects of energy-range relations, stopping power and energy straggling of protons. *Radiat Phys Chem*. 2007;76:1089–1107.
5. Kimstrand P, Traneus E, Ahnesjö A, Grusell E, Glimelius B, Tilly N. A beam source model for scanned proton beams. *Phys Med Biol*. 2007;52:3151–3168.
6. Wilkens JJ, Oelfke U. Analytical linear energy transfer calculations for proton therapy. *Med Phys*. 2003;30:806–815.
7. Marsolat F, De Marzi L, Pouzoulet F, Mazal A. Analytical linear energy transfer model including secondary particles: calculations along the central axis of the proton pencil beam. *Phys Med Biol*. 2016;61:740–757.
8. Sanchez-Parcerisa D, Cortés-Giraldo MA, Dolney D, Kondrla M, Fager M, Carabe A. Analytical calculation of proton linear energy transfer in voxelized geometries including secondary protons. *Phys Med Biol*. 2016;61:1705–1721.
9. Hirayama S, Matsuura T, Ueda H, et al. An analytical dose-averaged LET calculation algorithm considering the off-axis LET enhancement by secondary protons for spot-scanning proton therapy. *Med Phys*. 2018;45:3404–3416.
10. Bertolet A, Baratto-Roldán A, Barbieri S, Baiocco G, Carabe A, Cortés-Giraldo MA. Dose-averaged LET calculation for proton track segments using microdosimetric Monte Carlo simulations. *Med Phys*. 2019;46:4184–4192.
11. Bertolet A, Baratto-Roldán A, Cortés-Giraldo MA, Carabe-Fernandez A. Segment-averaged LET concept and analytical calculation from microdosimetric quantities in proton radiation therapy. *Med Phys*. 2019;46:4204–4214.
12. Berger MJ, Coursey JS, Zucker MA, Chang J. Stopping-Power; Range Tables for Electrons, Protons, and Helium Ions | NIST. NIST Standard Reference Database 124. https://www.nist.gov/pml/stopping-power-range-tables-electrons-protons-and-helium-ions. Published 2017. Accessed December 19, 2018.
13. ICRU. Report 90: Key Data for Ionizing Radiation Dosimetry: Measurement Standards and Applications. Vol 14; 2016.
14. Ulmer W, Matsinos E. Theoretical methods for the calculation of Bragg curves and 3D distributions of proton beams. *Eur Phys J Spec Top*. 2010;190:1–81.
15. Huang S, Kang M, Souris K, et al. Validation and clinical implementation of an accurate Monte Carlo code for pencil beam scanning proton therapy. *J Appl Clin Med Phys*. 2018;19:558–572.
16. Agostinelli S, Allison J, Amako K, et al. Geant4—a simulation toolkit. *Nucl Instrum Methods Phys Res Sect A Accel Spectrom Detect Assoc Equip*. 2003;506:250–303.
17. Allison J, Amako K, Apostolakis J, et al. Geant4 developments and applications. *IEEE Trans Nucl Sci*. 2006;53:270–278.
18. Allison J, Amako K, Apostolakis J, et al. Recent developments in Geant4. *Nucl Instrum Methods Phys Res Sect A Accel Spectrom Detect Assoc Equip*. 2016;835:186–225.
19. Grassberger C, Paganetti H. Elevated LET components in clinical proton beams. *Phys Med Biol*. 2011;56:6677–6691.
20. ICRU. *Report 16. Linear Energy Transfer*. Vol 9. Oxford University Press; 1970. https://doi.org/10.1093/jicru/os9.1.Report16
21. Varian Medical Systems. *Eclipse Scripting API Reference Guide*. Version 15; 2015.
22. Souris K, Lee JA, Sterpin E. Fast multipurpose Monte Carlo simulation for proton therapy using multi- and many-core CPU architectures. *Med Phys*. 2016;43:1700–1712.
23. Cortés-Giraldo MA, Carabe A. A critical study of different Monte Carlo scoring methods of dose average linear-energy-transfer maps calculated in voxelized geometries irradiated with clinical proton beams. *Phys Med Biol*. 2015;60:2645–2669.